Supporting Information

Determination of Acyl Chain positioning of Lipid A Isolated from *A. baumannii* LPS Using Tandem Mass Spectrometry.

The precursor ion at *m/z* 1910 corresponded to a lipid A structure that was diphosphoryl hepta-acylated (four primary fatty acids (two C12(3-OH) acyl chains and two C14(3-OH) acyl chains) and three secondary fatty acids (one C12(3-OH) acyl chain and two C12 acyl chains).

Figure S1 displays the dissociation mass spectrum (MS^2) of the ion at *m/z* 1910. Proposed structures for several diagnostic product ions observed in Figure S1 are presented in Scheme S1. The major dissociations of the precursor ion at *m/z* 1910 involved competitive and consecutive neutral loss(s) of phosphate (including both H_3PO_4 and HPO_3), C12, and C12(3-OH). For example, abundant product ions at *m/z* 1694, 1396 and 1196 in Figure S1a corresponded to neutral loss of [C12(3-OH)], [H_3PO_4, C12, and C12(3-OH)], and [H_3PO_4, two C12, and C12(3-OH)], respectively. Refer to Table S2 for identification of all other product ions. Note that loss of phosphoric acid could be a result of direct loss of H_3PO_4 or consecutive loss of HPO_3 and H_2O. Observation of high abundant product ions in the *m/z* region greater than 1190 clearly demonstrated the dominant fragmentation pathways upon gas-phase dissociation of lipid A anions involved neutral loss of fatty acids and/or phosphate leaving an intact negatively charged lipid A disaccharide backbone. Although these abundant product ions provided helpful insight into the composition of the fatty acids, they do not unambiguously assign acyl chains to specific locations.

Consequently, acyl chain positioning was determined by identifying cross-ring and glycosidic cleavages. Figure S1b shows the magnified *m/z* region of 850-1190 from Figure S1a. Here, we identified several cross-ring and glycosidic cleavages that allowed us to assign the fatty acids to specific locations. The product ions at *m/z* values 1184.7, 1104.7, and 904.6 represent a series of A-type product ions and were assigned the following designation: $^{0,4}A_2$ (2 HPO_3), $^{0,4}A_2$ (1 HPO_3), and $^{0,4}A_2$ (1 HPO_3)-C12, respectively. Next, a series of B-type

product ions at *m/z* values 1124.7, 1044.7, and 924.5 were observed and assigned the following designation: B_1 (2 HPO_3), B_1 (1 HPO_3), and B_1 (1 HPO_3)-C12, respectively. Finally, one reducing end glycosidic cleavage was observed at *m/z* 864.6 and corresponded to Y_1 (1 HPO_3). Cross-ring and glycosidic product ions were named following the nomenclature outlined by Costello *et al.* [1-3] with the slight modification of designating the number of phosphate groups present and loss of neutral acyl chains if applicable. The product ions at *m/z* 1184.7, 1124.7, and 924.5 contain two phosphate groups indicating the C-4′ position houses a pyrophosphate substituent. This observation was not unexpected given recent studies have demonstrated that diphosphorylated lipid A is a heterogeneous mixture of bisphosphate and pyrophosphate [4-5].

The A-type and B-type product ions allowed us to assign four acyl chains to the non-reducing end of the disaccharide backbone. These four fatty acids were determined to be two primary fatty acids (C12(3-OH) and C14(3-OH)) and two secondary fatty acids (C12(3-OH) and C12). The specific assignment of both the primary and secondary fatty acids was not completely attainable at the MS^2 stage but was achieved at the MS^3 stage (vide supra). Following deductive reasoning, if four of seven fatty acids are assigned to the non-reducing end of the lipid A disaccharide then the remaining three fatty acids are positioned at the reducing end of the disaccharide. This logic was substantiated by observation of the Y_1 product ion. Specific assignment outside of identifying two primary fatty acids (C12(3-OH) and C14(3-OH)) and one secondary fatty acid (C12) on the reducing end was not achieved via the MS^2 level of sophistication. Refer to Scheme S1 for proposed structures of the aforementioned of cross-ring and glycosidic cleavage product ions.

A series of MS^3 and MS^4 experiments originating from the dissociation of *m/z* 1910 were conducted in order to confidently assign acyl chain positions. The MS^3 dissociation mass spectrum of *m/z* 1694 (Figure S2) was highlighted as an example for acyl chain determination. The dissociation of *m/z* 1694 from *m/z* 1910 corresponded to the neutral loss of C12(3-OH). Here as was the case before, we relied on diagnostic product

ions resulting from cross-ring and glycosidic cleavages. The same series of A-type and B-type product ions (as well as their relative intensities) that were identified in the MS^2 mass spectrum of *m/z* 1910 (Figure S2) were also identified in the MS^3 mass spectrum of *m/z* 1694 (Figure S1). This strongly indicated the acyl chain lost giving rise to the product ion at *m/z* 1694 did not derive from the non-reducing end. Therefore, four fatty acids (two primary and two secondary) were left intact on the non-reducing end in the product ion *m/z* 1694. In order to determine the fatty acid positions on the non-reducing end, we followed the consecutive dissociation of the ion at *m/z* 1104.7 ($^{0,4}A_2$ (1 HPO_3)).

First, we saw the loss of C12 at *m/z* 904.8. Non-hydroxylated fatty acids are almost entirely secondary fatty acids and this held true for lipid A from *A. baumannii*. Next, the consecutive/competitive loss of C12:1 (ketene) and C12:1 demonstrated the second fatty acid lost resulting in *m/z* values 724.7 and 706.7 were from a primary ester-linked fatty acid. In other words, the C-3′ position contained a primary C12(3-OH) acyl chain and a secondary C12 acyl chain. As is customary with all secondary fatty acids they are ester-linked to the 3-hydroxy position of the primary 3-hydroxy fatty acid [6]. The rationale for the aforementioned conclusion was explained as follows: 1) The first acyl chain loss (C12) was from a secondary position given the non-reducing end had four fatty acids of which only two can be primary fatty acids which by default assigns the other two as secondary fatty acids. A primary fatty acid can not be lost prior to losing a secondary fatty acid if both primary fatty acids contain a secondary fatty acid. Consequently, the first fatty acid lost must be a secondary fatty acid. Also, primary fatty acids are known to be almost exclusively hydroxylated [6].; 2) Neutral loss of the secondary fatty acid resulting from gas-phase dissociation give rise to a primary fatty acid with one point of unsaturation. Next, ester-linked fatty acids are more labile then their amide-linked counterparts leading to preferential loss of ester-linked over amide-linked primary fatty acids. The non-reducing end contains a primary ester-linked fatty acid at position C-3′ and a primary amide-linked fatty acid at position C-2′. Therefore, the C12 secondary fatty acid and the C12(3-OH) primary fatty acid are situated at the C-3′ position.

The C-2′ position was determined to have the following arrangement: primary amide-linked C14(3-OH) acyl chain and secondary C12(3-OH) acyl chain. This assignment was achieved by observation of the ion at *m/z* 688.6 which corresponded to $^{0,4}A_2$ (1 HPO_3)-C12-C12(3-OH). Additionally, lack of neutral loss of C14(3-OH) from any of the product ions in (Figure S2) is an major indication that C14(3-OH) is a primary amide-linked fatty acid. This observation is contrary to previous reports [7,8] which proposed the C-2′ position has a primary amide-linked C12(3-OH) and a secondary ester-linked C14(3-OH).

As mentioned previously, the reducing end of the lipid A disaccharide contained three fatty acids of which two are primary fatty acids (C14(3-OH) and C12(3-OH)) and remaining fatty acid is a C12 secondary acyl chain. The neutral loss of C12(3-OH) from the ion at *m/z* 1910 giving rise to the ion at *m/z* 1694 is assigned as a primary fatty acid attached at the C-3 position. This can be explained as follows: C12 is a secondary fatty acid and must be attached to either the C-2 or C-3 primary fatty acid. We also know that the C12(3-OH) primary fatty acid cannot contain the secondary C12 acyl chain. Furthermore, the ester-linked primary fatty acid at C-3 will be preferentially cleaved over the C-2 amide-linked primary fatty acid. This localized the C12(3-OH) primary fatty acid to the C-3 position and consequently puts the C14(3-OH) primary fatty acid and C12 secondary fatty acid on the C-2 position. This acylation pattern was further confirmed with the observation of Y_1 (1 HPO_3) not containing C12(3-OH) (Figure S2).

The acyl chain configuration as outlined above held true for all hepta-acylated lipid A extracted from *A. baumannii.* Refer to inset in Figure 1 for proposed structure of hepta-acylated lipid A extracted from *A. baumannii*.

Identification and localization of phosphoethanolamine (pEtN) addition to Lipid A Isolated from *A. baumannii* LPS Using Tandem Mass Spectrometry.

Tandem mass spectrometric experiments on the precursor ion at *m/z* 2033, which corresponded to the addition of a pEtN substituent to hepta-acylated lipid A were carried out in turn to correctly identify and localize the pEtN modification. Initial characterization based on elemental composition from accurate mass measurements of the hepta-acylated plus the 123 mass unit modification precursor ion at *m/z* 2033 revealed the composition of the 123 mass unit modification to be pEtN ($C_2H_6NPO_3$; accurate mass = 123.0085; experimental mass = 123.0161; 7.6 mmu). The pEtN modification has been reported previously yet decisive evidence for localizing the pEtN group has been vague. In order to determine the location of the pEtN modification we conducted a series of tandem mass spectrometric experiments aimed at highlighting diagnostic product ions that provided convincing evidence for localizing the pEtN substituent.

Gas-phase dissociation of the precursor ion at *m/z* 2033 resulting in the generation of a MS^2 mass spectrum is highlighted in Figure S3. The overwhelming dissociation pathway from the precursor ion at *m/z* 2033 involved the neutral loss of the pEtN group at *m/z* 1910. The ion at *m/z* 1910 corresponded to diphosphoryl hepta-acylated lipid A (refer to the previous section for phosphate and acyl chain assignments). In addition to the abundant ion at *m/z* 1910, a series of more modest abundant product ions resulting from competitive and consecutive neutral loss(s) from pEtN, fatty acids, and phosphate were present. These ions provided insightful information regarding the acyl chain and phosphate configuration however did not yield conclusive evidence for pEtN assignment. pEtN localization was achieved via examination of product ions resulting from cross-ring and glycosidic cleavages.

Close examination of the *m/z* region 700-1250 (Figure S3) displayed several diagnostic cross-ring and glycosidic product ions. Here, the identified cross-ring and glycosidic cleavages that allowed us to assign the pEtN to specific locations. The product ion at *m/z* value 1227.7 represented an A-type product ion and was

assigned the following designation: $^{0,4}A_2$ [w/pEtN]. Next, a series of B-type product ions at *m/z* values 1167.7, 951.6, and 751.4 were observed and assigned the following designation: B_1 [w/pEtN], B_1-C12(3-OH) [w/pEtN], B_1-C12(3-OH)-C12 [w/pEtN], respectively. Additionally, one reducing end glycosidic cleavage was observed at *m/z* 987.6 and corresponded to Y_1 [w/pEtN]. Refer to Scheme S1 for proposed structures of product ions. The aforementioned diagnostic product ions allowed us to assign the pEtN modification to both the reducing and non-reducing end of the lipid A disaccharide backbone. Moreover, the pEtN group was found to be attached to the lipid A backbone via a phosphodiester bond at either the C-4' monophosphate or the C-1 monophosphate position. At this level of MS sophistication, we did not observe pEtN attached directly to a pyrophosphate group or pEtN attached without linkage to the C-4' or C-1 monophosphate group. The presence of pyrophosphate in the structure corresponding to *m/z* value 2033 was confirmed in the IRMPD MS^2 mass spectrum of the ion at *m/z* 2033 (data not shown). A previous report [5] estimated the abundance of pyrophosphorylated lipid A extracted from *Yersinia pestis* LPS to be near 5%. Equally apparent from this report was the vast majority (~95%) of diphosphorylated lipid A comprised of a bisphosphorylated configuration. Therefore, assuming *A. baumannii* lipid A is consistent with the general notion that it is predominately composed of bisphosphate combined with the inability to sufficiently characterize pyrophosphorylated lipid A from *A. baumannii*, we focused our efforts on characterizing the PEtN modification in context with bisphosphorylated *A. baumannii* lipid A.

Localization of the glycan addition to Lipid A Isolated from *A. baumannii* LPS Using Tandem Mass Spectrometry.

Tandem mass spectrometric experiments on the precursor ion at *m/z* 2071, which corresponded to the addition of a hexosamine group to hepta-acylated lipid A were carried out in order to clearly localize the glycan modification. Initial characterization based on elemental composition from accurate mass measurements of the

hepta-acylated plus the 161 mass unit modification precursor ion at *m/z* 2071 revealed the composition of the 161 mass unit modification to be a hexosamine group ($C_6H_{11}NO_4$; accurate mass = 161.0688; experimental mass = 161.0598; mass difference = 9.0 mmu). The glycan modification has not been reported previously. A series of tandem mass spectrometric experiments aimed at highlighting diagnostic product ions that provided convincing evidence for localizing the glycan modification were conducted.

Gas-phase dissociation of the precursor ion at *m/z* 2071 resulting in the generation of a MS^2 mass spectrum is highlighted in Figure S4. The overwhelming dissociation pathway from the precursor ion at *m/z* 2071 involved the neutral loss of the hexosamine group at *m/z* 1910. The ion at *m/z* 1910 corresponded to diphosphoryl hepta-acylated lipid A (refer above for phosphate and acyl chain assignments). In addition to the abundant ion at *m/z* 1910, a series of more modest abundant product ions resulting from competitive and consecutive neutral loss(s) from the hexosamine, fatty acids, and phosphate were present. These ions provided insightful information regarding the acyl chain and phosphate configuration however did not yield conclusive evidence for the glycan assignment. Glycan localization was achieved via examination of product ions resulting from glycosidic cleavages.

We identified several glycosidic cleavages that allowed us to assign the glycan modification to the reducing end of the lipid A disaccharide. The product ions at *m/z* values 1025.6 and 864.6 represented Y-type product ions and were assigned the following designation: Y_1 [w/ Hex] and Y_1-Hex. Absence of non-reducing end product ions further substantiated the claim that the hexosamine modification was located at the C-1 position. Refer to Scheme S2 for proposed structures of product ions. The aforementioned diagnostic product ions allowed us to assign the glycan modification to the reducing end of the lipid A disaccharide backbone. Moreover, the glycan group was found to be attached to the lipid A backbone via a phosphodiester bond at the C-1 monophosphate position. At this level of MS sophistication, we did not observe the glycan attached directly to a pyrophosphate group or attached without linkage to the C-1 monophosphate group. The presence of

pyrophosphate in the structure corresponding to *m/z* value 2071 was confirmed in the IRMPD MS^2 mass spectrum of the ion at *m/z* 2071 (data not shown). A previous report [5] estimated the abundance of pyrophosphorylated lipid A extracted from *Yersinia pestis* LPS to be near 5%. Equally apparent from this report was the vast majority (~95%) of diphosphorylated lipid A comprised of a bisphosphorylated configuration. Therefore, assuming *A. baumannii* lipid A is consistent with the general notion that it is predominately composed of bisphosphate combined with the inability to sufficiently characterize pyrophosphorylated lipid A from *A. baumannii*, we focused our efforts on characterizing the hexosamine modification in context with bisphosphorylated *A. baumannii* lipid A.

Assignment of both the phosphoethanolamine (pEtN) and glycan modifications to Lipid A Isolated from A. baumannii LPS Using Tandem Mass Spectrometry.

Tandem mass spectrometric experiments on the precursor ion at *m/z* 2194, which corresponded to the addition of both pEtN and hexosamine substituents to hepta-acylated lipid A were performed to correctly identify and localize the pEtN and hexosamine modifications. Initial characterization based on elemental composition from accurate mass measurements of the hepta-acylated plus the 123 and 161 mass unit modifications at *m/z* 2194 revealed the composition of the 123 mass unit modification to be pEtN ($C_2H_6NPO_3$; accurate mass = 123.0085; experimental mass = 123.0001; 8.4 mmu) and the 161 mass unit modification to be hexosamine ($C_6H_{11}NO_4$; accurate mass = 161.0688; experimental mass = 161.0620; mass difference = 6.8 mmu). The combined pEtN and hexosamine modifications have not been reported. In order to determine the location of the pEtN and hexosamine modifications we conducted a series of tandem mass spectrometric experiments aimed at highlighting diagnostic product ions that provided convincing evidence for localizing the two substituents.

Gas-phase dissociation of the precursor ion at *m/z* 2194 resulting in the generation of a MS^2 mass spectrum is highlighted in Figure S5. The overwhelming dissociation pathway from the precursor ion at *m/z*

2094 involved the neutral loss of both the pEtN and hexosamine group at *m/z* 1910. The ion at *m/z* 1910 corresponded to diphosphoryl hepta-acylated lipid A (sans pEtN and hexosamine). In addition to the abundant ion at *m/z* 1910, numerous other less abundant product ions were observed resulting from competitive and consecutive neutral loss(s) from the pEtN, hexosamine, fatty acids, and phosphate. These ions provided discerning information regarding the acyl chain and phosphate configuration however did not yield vital evidence for PEtN and hexosamine assignment. pEtN and hexosamine localization was achieved via examination of product ions resulting from glycosidic cleavages.

We identified several glycosidic cleavages in Figure S5 that allowed us to assign the pEtN to the non-reducing end and the hexosamine to the reducing end of the disaccharide backbone. The product ions at *m/z* value 951.5 and 751.4, represented a series of B-type product ions and were assigned the following designations: B_1-C12(3-OH) [w/pEtN] and B_1-C12(3-OH)-C12 [w/pEtN], respectively. Also, the product ions at *m/z* values 1025.6, 864.6, and 664.4 represented a series of Y-type product ions and were assigned the following designation: Y_1 [w/ Hex] and Y_1-Hex, and Y_1-Hex-C12, respectively. Refer to Scheme S3 for proposed structures of product ions. The aforementioned diagnostic product ions allowed us to confidently assign the pEtN modification to the non-reducing end and the hexosamine modification to the reducing end of the lipid A disaccharide backbone. Moreover, both modifications were found to be attached to the lipid A backbone via a phosphodiester bond at the C-4' monophosphate position for pEtN and at the C-1 monophosphate position for hexosamine. At this level of MS sophistication, we did not observe pEtN or hexosamine attached directly to a pyrophosphate group and pEtN or hexosamine attached without linkage to the C-4' or C-1 monophosphate group, respectively. The presence of pyrophosphate in the structure corresponding to *m/z* 2194 was confirmed in the IRMPD MS^2 mass spectrum of the ion at *m/z* 2194 (data not shown). A previous report [5] estimated the abundance of pyrophosphorylated lipid A extracted from *Yersinia pestis* LPS to be near 5%. Equally apparent from this report was the vast majority (~95%) of diphosphorylated lipid A

comprised of a bisphosphorylated configuration. Therefore, assuming *A. baumannii* lipid A is consistent with the general notion that it is predominately composed of bisphosphate combined with the inability to sufficiently characterize pyrophosphorylated lipid A from *A. baumannii*, we focused our efforts on characterizing the PEtN and hexosamine modifications in context with bisphosphorylated *A. baumannii* lipid A.

REFERENCES

1. **Domon B, Costello CE.** 1988. Systematic Nomenclature for Carbohydrate Fragmentations in FAB-MS/MS Spectra of Glycoconjugates. Glycoconjugate. **5**:397-409.
2. **Costello CE, Vath JE.** 1990. Tandem Mass Spectrometry of Glycolipids. Methods Enzymol. **193**:738–768.
3. **Domon B, Vath JE, Costello CE.** 1990. Analysis of Derivatized Ceramides and Neutral Glycosphinogolipids by High-performance Tandem Mass Spectrometry. Anal. Biochem. **184**:151-164.
4. **Jones JW, Shaffer SA, Ernst RK, Goodlett DR, Turecek F.** 2008. Determination of pyrophosphorylated forms of lipid A in Gram-negative bacteria using a multivaried mass spectrometric approach. PNAS. **105**: 12742-12747.
5. **Jones JW, Cohen IE, Turecek F, Goodlett DR, Ernst RK.** 2010. Comprehensive Structure Characterization of Lipid A Extracted from *Yersinia pestis* for Determination of its Phosphorylation Configuration. J. Am. Soc. Mass Spectrom. **21**:785-799.
6. **Raetz CR, Whitfield C.** 2002. Lipopolysaccharide Endotoxins. Annu. Rev. Biochem. **71**:635–700
7. **Beceiro A, Llobet E, Aranda J, Bengoechea JA, Doumith M, Hornsey M, Dhanji H, Chart H, Bou G, Livermore DM, Woodford N.** 2011. Phosphoethanolamine Modification of Lipid A in Colistin-Resistant Variants of *Acinetobacter baumannii* Mediated by the *pmrAB* Two-Component Regulatory System. Antimicrob. Agents Chemother. **55**:3370-3379.
8. **Arroyo LA, Herrera CM, Fernandez L, Hankins JV, Trent MS, Hancock REW.** 2011. The *pmrCAB* Operon Mediates Polymyxin Resistance in *Acinetobacter baumannii* ATCC 17978 and Clinical Isolates through Phosphoethanolamine Modification of Lipid A. **55**:3743-3751.

FIGURE CAPTIONS – SUPPLEMENTAL INFORMATION

Supporting Information (SI)

Figure/Scheme Captions

Figure S1. Negative ion mode ESI LTQ CID MS^3 mass spectrum of the precursor ion at *m/z* 1694. Inset structure displays proposed configuration for ion at *m/z* 1694 with dashed lines across likely bond cleavage sites. Dashed lines at C-1 and C-4′ positions labeled with an "X" indicate multiple phosphorylation configuration (i.e., C-1 and C-4′ bisphosphate, C-1 pyrophosphate, and C-4′ pyrophosphate). Nomenclature associated with each *m/z* value indicates neutral loss(s) or glycosidic/cross-ring designation. Inset mass spectrum shows highlighted *m/z* region 600-1100.

Figure S2. Fatty acid analysis via GC-FID displayed via percentage of fatty present to total fatty acids.

Figure S3. Negative ion mode ESI FT-ICR CID MS^2 mass spectrum of the precursor ion at *m/z* 2033. Inset structure displays proposed bis-phosphorylated configuration for ion at *m/z* 2033 with dashed lines across likely bond cleavage sites. The pEtN modification was determined to be situated at either the C-1 or C-4′ position monophosphate. Nomenclature associated with each *m/z* value indicates neutral loss(s) or glycosidic/cross-ring designation.

Figure S4. Negative ion mode ESI FT-ICR CID MS^2 mass spectrum of the precursor ion at *m/z* 2071. Inset structure displays proposed bis-phosphorylated configuration for ion at *m/z* 2071 with dashed lines across likely bond cleavage sites. The hexosamine modification was determined to be located

exclusively at the C-1 position monophosphate. Nomenclature associated with each *m/z* value indicates neutral loss(s) or glycosidic/cross-ring designation.

Figure S5. Negative ion mode ESI FT-ICR CID MS^2 mass spectrum of the precursor ion at *m/z* 2194. Inset structure displays proposed bis-phosphorylated configuration for ion at *m/z* 2194 with dashed lines across likely bond cleavage sites. The pEtN and hexosamine modifications were determined to be located at the C-4′ and C-1 position monophosphates, respectively. Nomenclature associated with each *m/z* value indicates neutral loss(s) or glycosidic/cross-ring designation.

Scheme S1. A) Proposed structures for precursor ion at *m/z* 1910 and its associated glycosidic and cross-ring product ions. B) Proposed structures for precursor ion at *m/z* 2033 and its associated glycosidic and cross-ring product ions.

Scheme S2. Proposed structures for precursor ion at *m/z* 2071 and its associated glycosidic product ions.

Scheme S3. Proposed structures for precursor ion at *m/z* 2194 and its associated glycosidic product ions.

Table S1. Descriptive Information of *A. baumannii* clinical isolates.

Table S2. Product ions resulting from gas-phase dissociation of precursor ion at *m/z* 1910.

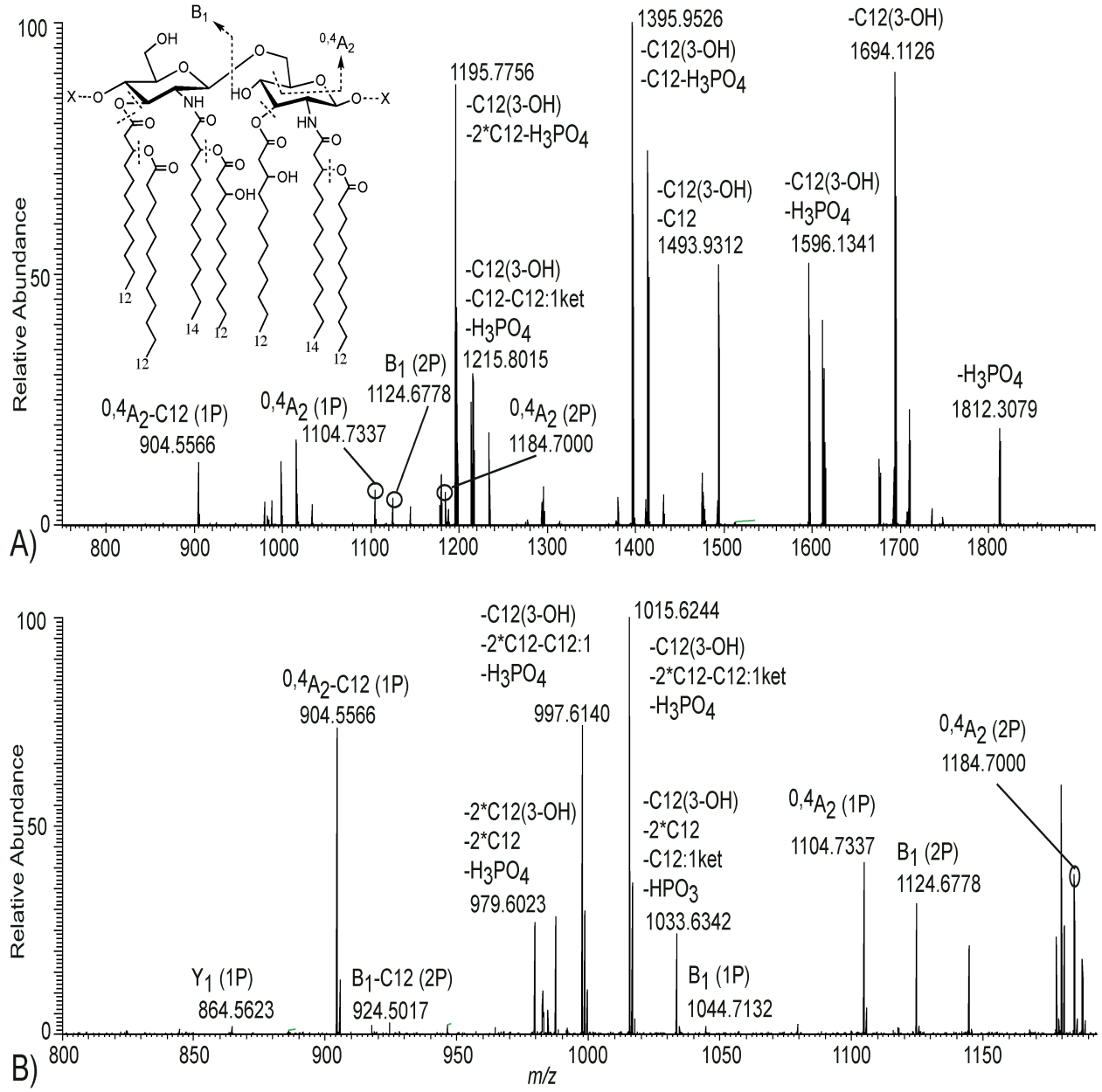

Figure S1 – Pelletier et al

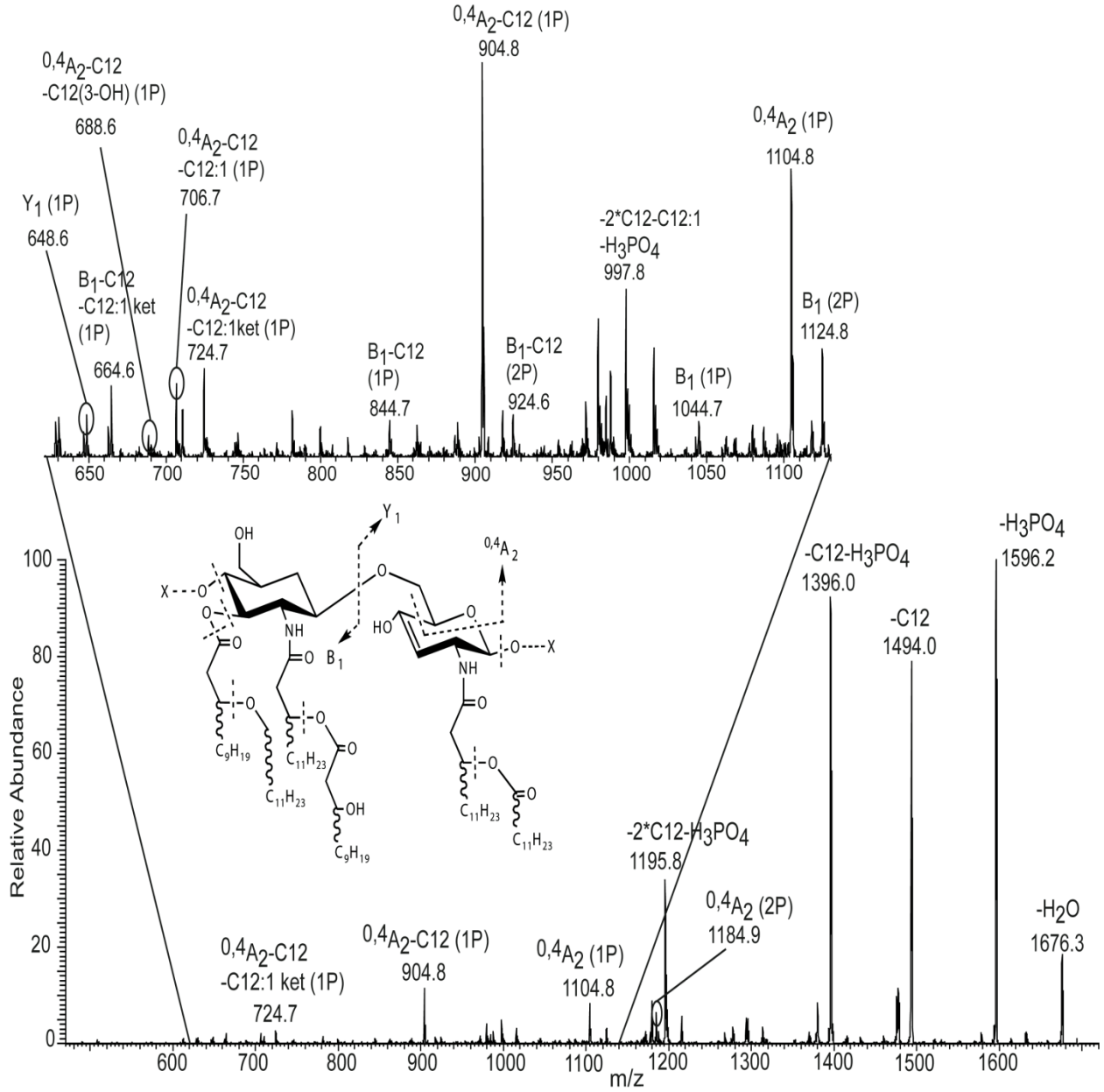

Figure S2 – Pelletier et al

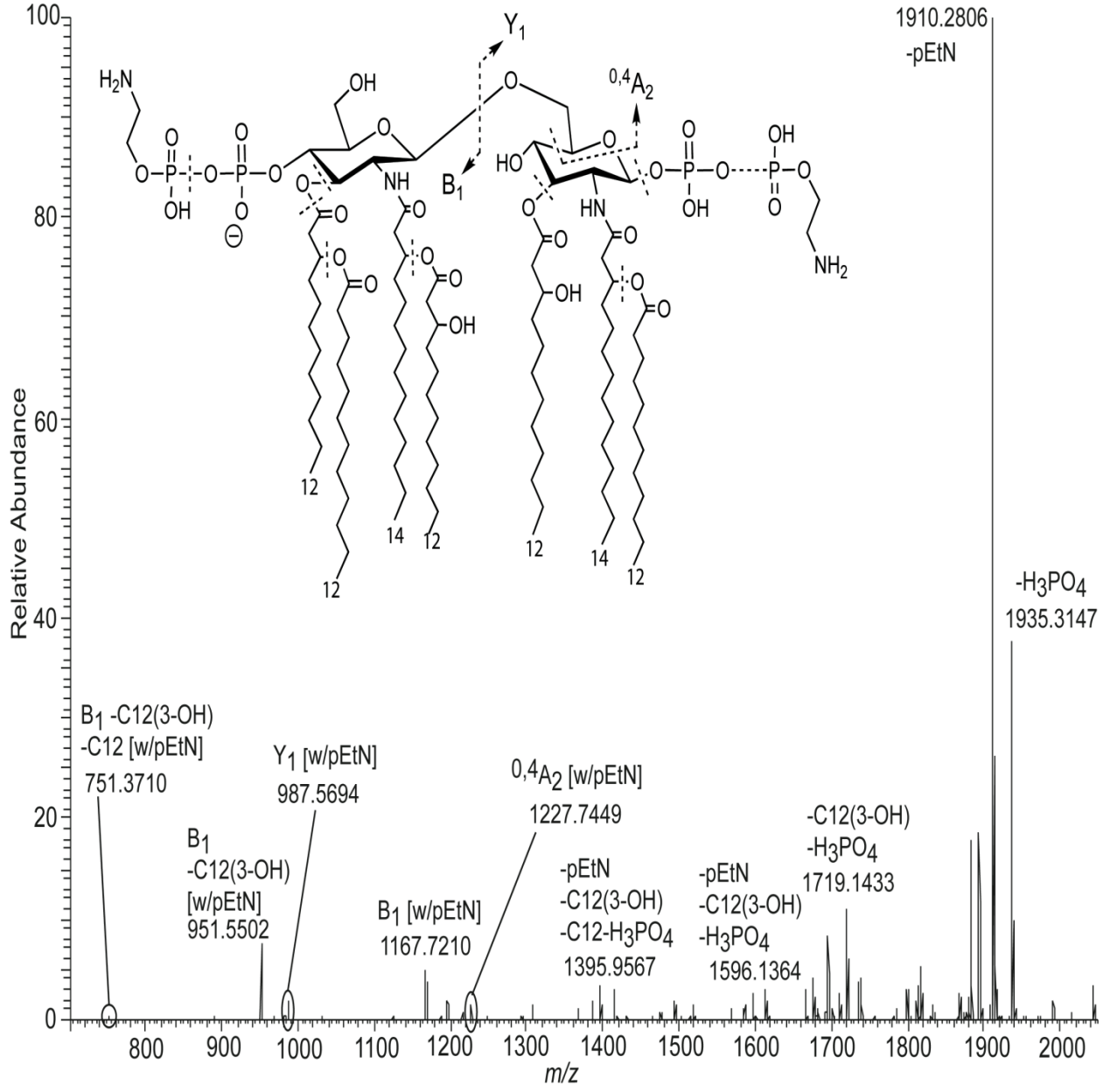

Figure S3– Pelletier et al

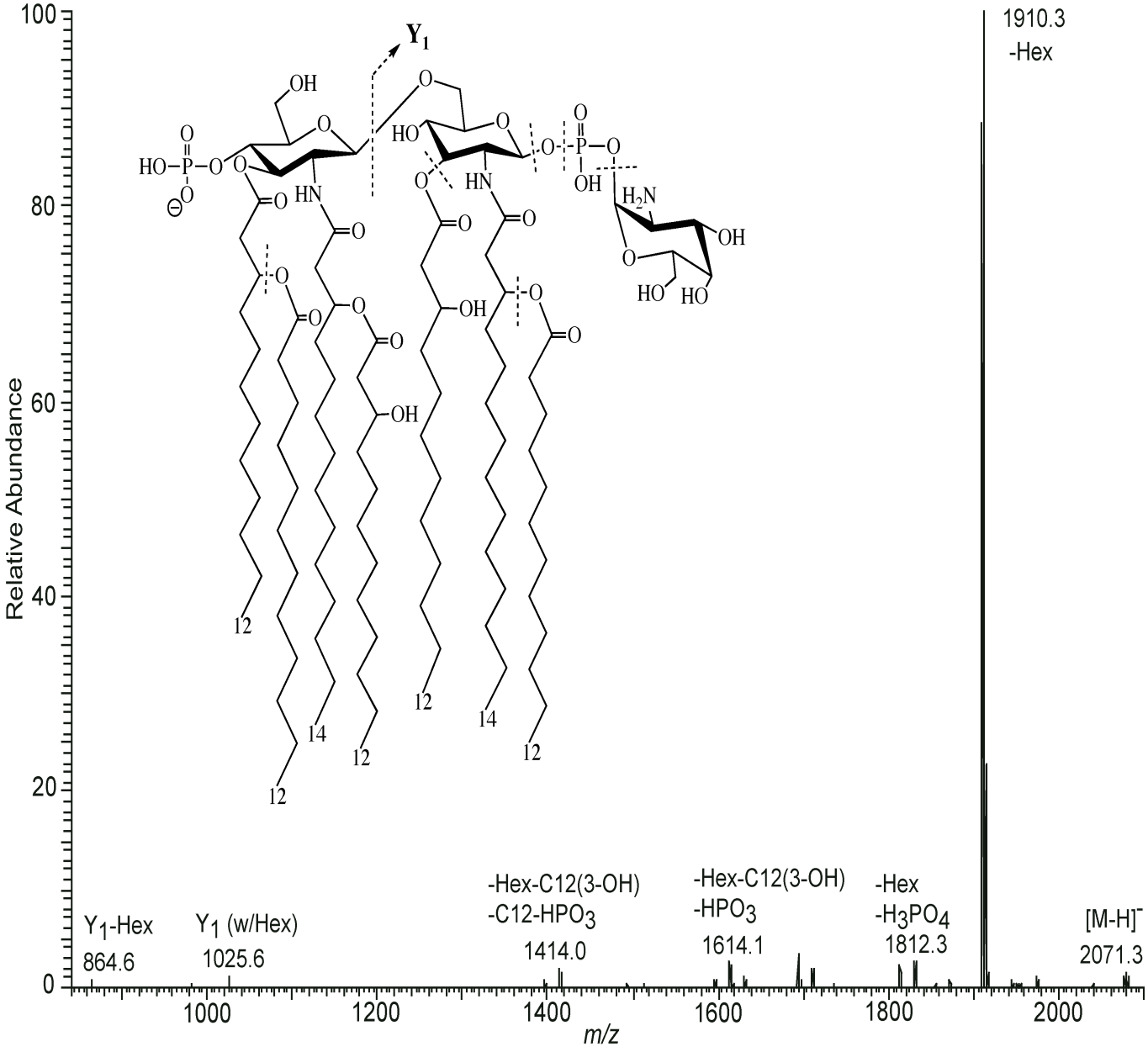

Figure S4 – Pelletier et al

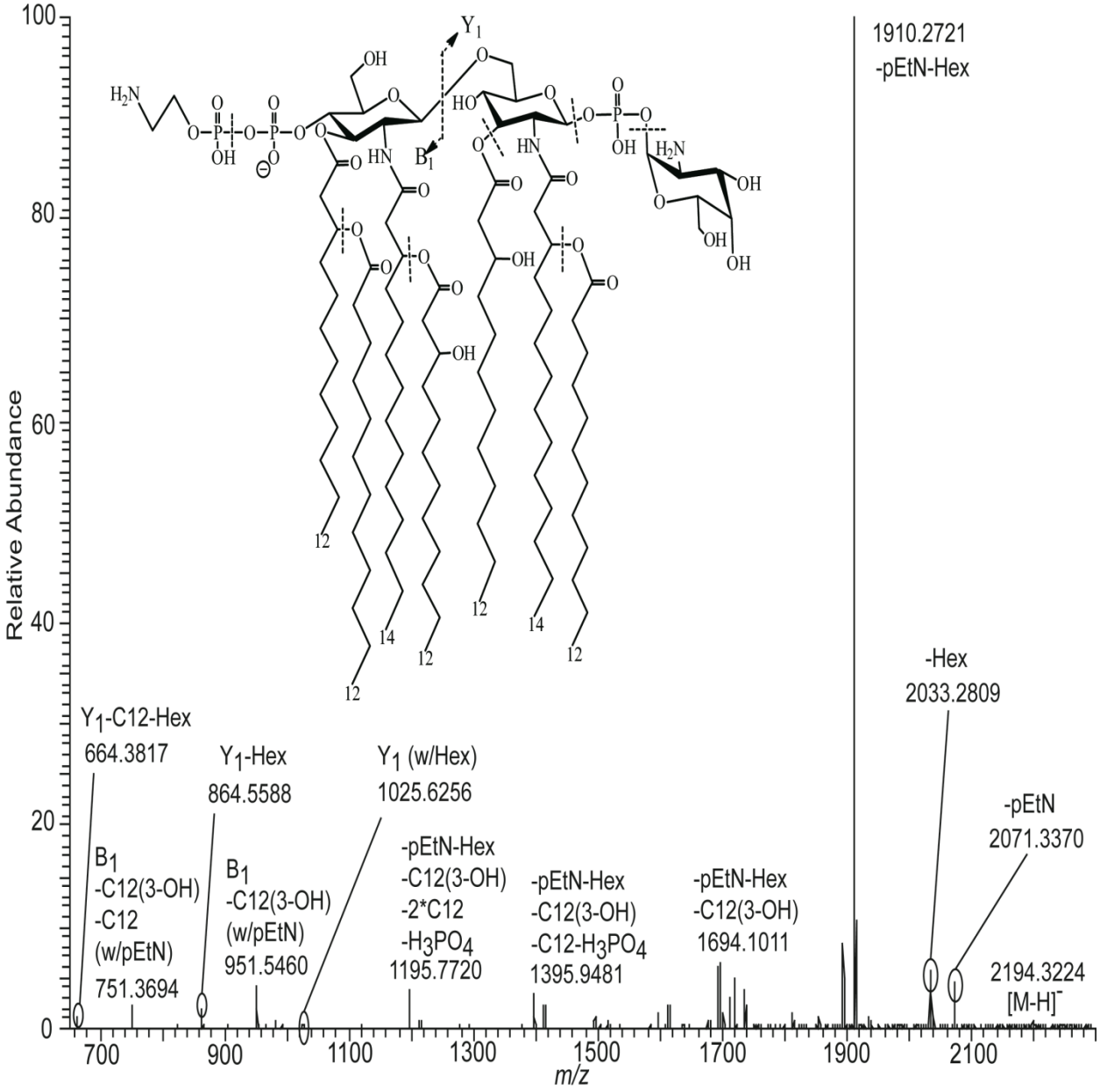

Figure S5 – Pelletier et al

A

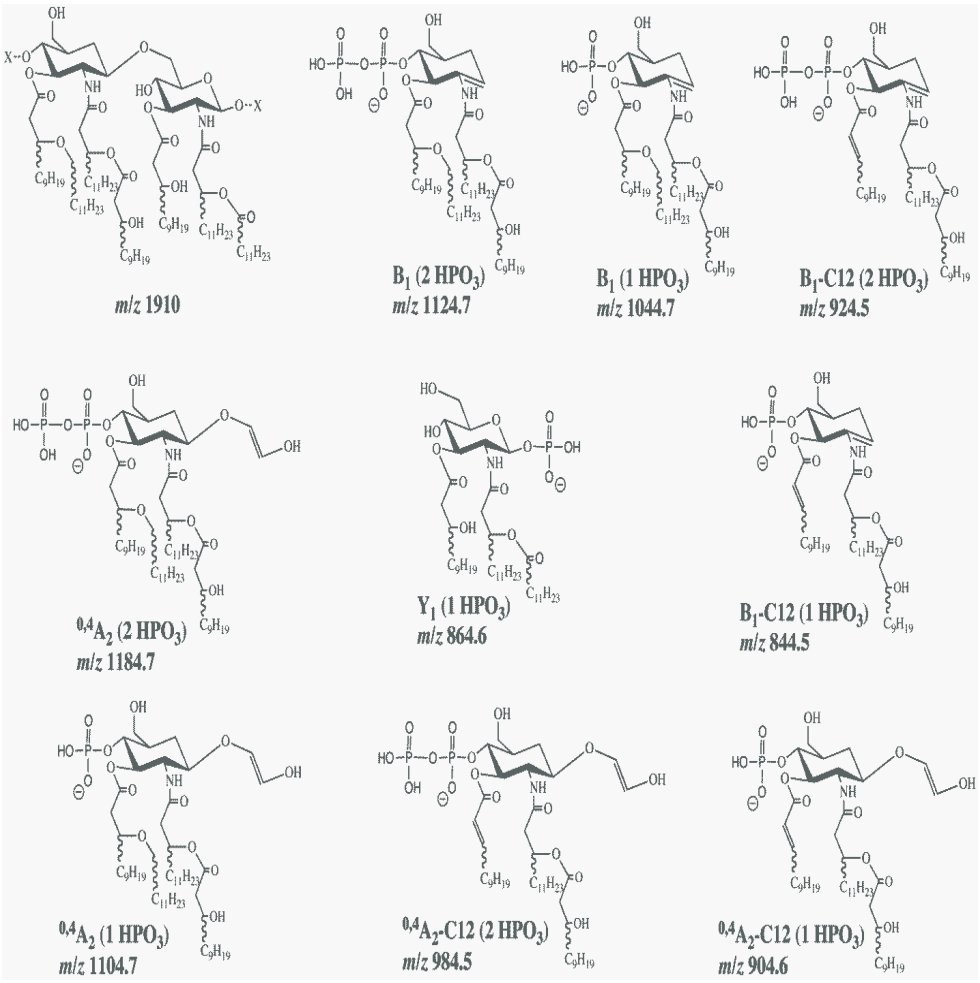

B

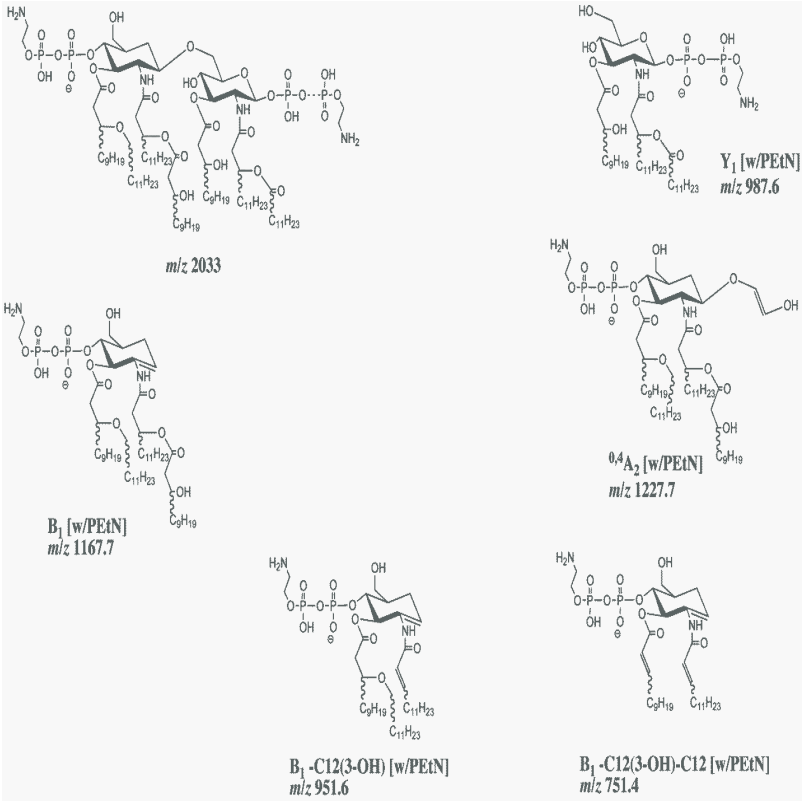

Scheme S1-Pelletier et al

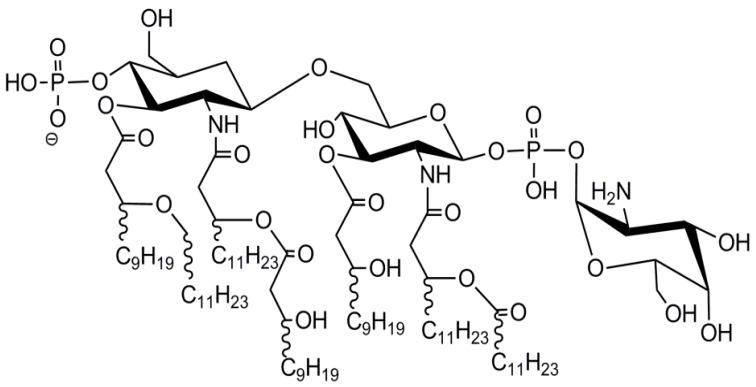

***m/z* 2071**

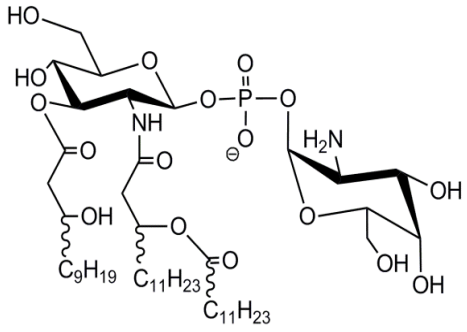

Y_1 [w/Hex]
***m/z* 1025.6**

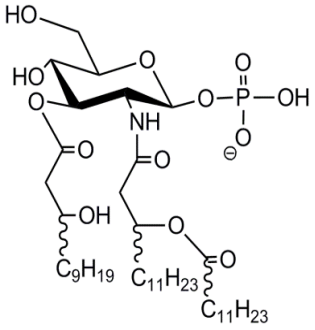

Y_1 - Hex
***m/z* 1025.6**

Scheme S2-Pelletier et al

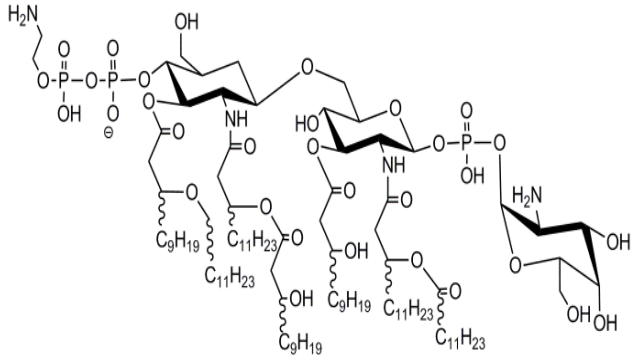

***m/z* 2194**

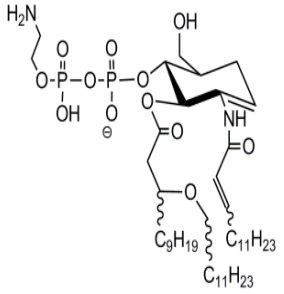

B_1 -C12(3-OH) [w/PEtN]
***m/z* 951.6**

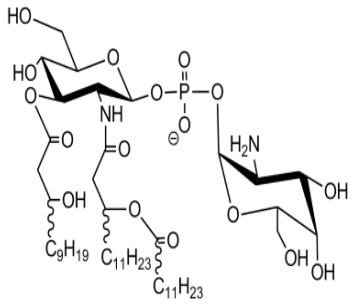

Y_1 [w/Hex]
***m/z* 1025.6**

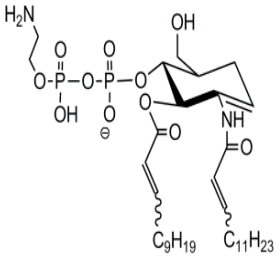

B_1 -C12(3-OH)-C12 [w/PEtN]
***m/z* 751.4**

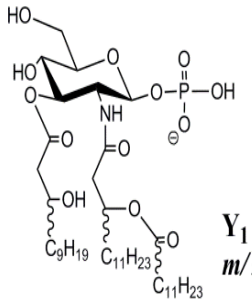

Y_1 -Hex
***m/z* 864.6**

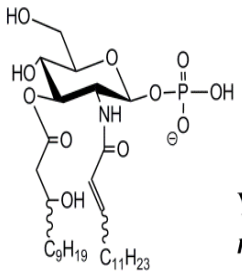

Y_1 -Hex-C12
***m/z* 664.4**

Supplemental Table 1. Acinetobacter baumannii clinical isolates

Species	Sample # [1]	Date of Collection	Source
A. baumannii	1494	1/9/07	Bronchoalveolar lavage
A. baumannii	1508	1/24/07	Sputum
A. baumannii	2382	8/17/09	Bronchoalveolar lavage
A. baumannii	2384	8/21/09	Sputum
A. baumannii	2949	2/5/11	Bronchoalveolar lavage
A. baumannii	2949A	2/16/11	Bronchoalveolar lavage

[1] Isolates 1494 and 1508, 2382 and 2384, and 2949 and 2949A were collected from the same patients, respectively

Supplemental Table 2. Product ions resulting from gas-phase dissociation of precursor ion at *m/z* 1910.

Structure	Experimental *m/z*	Theoretical *m/z*	Mass Accuracy (mmu)	Mass Accuracy (ppm)
[M-2*C12(3-OH)-2*C12-C12:1ket - H3PO4]-	799.4537	799.4515	2.2	2.8
B1-C12; 1 HPO3	844.5351	844.5345	0.6	0.7
Y1; 1 HPO3	864.5623	864.5608	1.5	1.7
0,4A2-C12; 1 HPO3	904.5566	904.5557	0.9	1.0
B1-C12; 2 HPO3	924.5017	924.5009	0.8	0.9
[M-C12(3-OH)-2*C12-C12:1-H3PO4-H2O]-	979.6023	979.6030	-0.7	-0.7
0,4A2-C12; 2 HPO3	984.5223	984.5223	0.0	0.0
[M-C12(3-OH)-2*C12-C12:1-H3PO4]-	997.6140	997.6135	0.5	0.5
[M-C12(3-OH)-2*C12-C12:1ket-H3PO4]-	1015.6244	1015.6241	0.3	0.3
[M-C12(3-OH)-2*C12-C12:1ket-HPO3]-	1033.6342	1033.6346	-0.4	-0.4
B1; 1 HPO3	1044.7132	1044.7122	1.0	1.0
0,4A2; 1 HPO3	1104.7337	1104.7333	0.4	0.4
B1; 2 HPO3	1124.6778	1124.6785	-0.7	-0.6
[M-C12(3-OH)-2*C12-H3PO4-H2O]-	1177.7650	1177.7649	0.1	0.1
[M-C12(3-OH)-C12-C12:1-H3PO4-H2O]-	1179.7806	1179.7806	0.0	0.0
0,4A2; 2 HPO3	1184.7000	1184.6996	0.4	0.3
[M-C12(3-OH)-2*C12-H3PO4]-	1195.7756	1195.7755	0.1	0.1
[M-C12(3-OH)-C12-C12:1-H3PO4]-	1197.7910	1197.7911	-0.1	-0.1
[M-C12(3-OH)-2*C12-HPO3]-	1213.7862	1213.7861	0.1	0.1
[M-C12(3-OH)-C12-C12:1ket-H3PO4]-	1215.8016	1215.8017	-0.1	-0.1
[M-C12(3-OH)-C12-C12:1ket-HPO3]-	1233.8124	1233.8124	0.0	0.0
[M-2*C12(3-OH)-C12:1]-	1277.7575	1277.7575	0.0	0.0
[M-C12(3-OH)-2*C12:1]-	1293.7527	1293.7524	0.3	0.2
[M-C12(3-OH)-C12-C12:1]-	1295.7682	1295.7680	0.2	0.2
[M-C12(3-OH)-C12-C12:1ket]-	1313.7751	1313.7786	-3.5	-2.7
[M-2*C12(3-OH)-H3PO4]-	1379.9579	1379.9582	-0.3	-0.2
[M-C12(3-OH)-C12-H3PO4]-	1395.9526	1395.9531	-0.5	-0.4
[M-2*C12-H3PO4]-	1411.9449	1411.9480	-3.1	-2.2
[M-C12-C12:1-H3PO4]-	1413.9642	1413.9637	0.5	0.4
[M-C12-C12:1ket-H3PO4]-	1431.9756	1431.9743	1.3	0.9
[M-C12(3-OH)-C12-H2O]-	1475.9199	1475.9195	0.4	0.3
[M-C12(3-OH)-C12]-	1493.9312	1493.9300	1.2	0.8
[M-C12(3-OH)-H3PO4]-	1596.1341	1596.1308	3.3	2.1
[M-C12-H3PO4]-	1612.1295	1612.1257	3.8	2.4
[M-C12(3-OH)-H2O]-	1676.1003	1676.0971	3.2	1.9
[M-C12(3-OH)]-	1694.1126	1694.1077	4.9	2.9
[M-C12]-	1710.1081	1710.1026	5.5	3.2
[M-H3PO4]-	1812.3079	1812.3033	4.6	2.5